An Empirical Study of the Performance of APMOVPE AM0 InP Homojunction Solar Cells as a Function of Emitter Thickness and Doping, and Base Doping

M. W. Wanlass, T. A. Gessert, K. A. Emery and T. J. Coutts

Solar Energy Research Institute
1617 Cole Blvd.
Golden, CO 80401

Introduction

Their excellent radiation resistance [ref. 1] and conversion efficiencies $> 20\%$, measured under global conditions [ref. 2], make InP shallow-homojunction solar cells very attractive for space or terrestrial application. In addition, modeling studies [ref. 3] show that, for optimized design, efficiencies of these devices should exceed 20% even under AM0 conditions. However, a systematic experimental investigation of the influence of the various cell design parameters on cell performance has not as yet been made. For the $n^+/p/p^+$ structures investigated in the previous modeling study, the design parameters include the impurity concentrations and thicknesses of the emitter and base layers. In the work reported here, we discuss an experimental investigation of the effects on cell performance of varying the impurity concentrations of the emitter and base and thickness of the emitter.

Shallow-Homojunction Solar Cell Structure

A schematic cross-section of the InP shallow homojunction structure under investigation is shown in Figure 1. The structure consists of a single-crystal p^+-InP substrate upon which are deposited three successive homoepitaxial layers of InP. These include a 0.5 μm p^+ buffer layer with an impurity concentration of $5 \times 10^{18} cm^{-3}$, a 3 μm p-type base layer with a variable impurity concentration and an emitter layer with variable thickness and impurity concentration. A study of photovoltaic performance vs cell design was carried out by systematically varying each of the emitter thickness, base doping and emitter doping while holding the other two parameters at constant values. Thus, the emitter thickness was varied from 100Å to 700Å while holding the base doping at $4 \times 10^{16} cm^{-3}$ and the emitter doping at $4 \times 10^{18} cm^{-3}$, the base doping was varied from $3 \times 10^{15} cm^{-3}$ to $3 \times 10^{17} cm^{-3}$ while holding the emitter doping at $4 \times 10^{18} cm^{-3}$ and the emitter thickness at 400Å and the emitter doping was varied from $6 \times 10^{17} cm^{-3}$ to $4 \times 10^{18} cm^{-3}$ while holding the base doping constant at $4 \times 10^{16} cm^{-3}$ and the emitter thickness at 700Å. For the emitter doping variation, the doping was spiked to $4 \times 10^{18} cm^{-3}$ over the last 150Å of the emitter (i.e., near the surface) to facilitate formation of an ohmic grid contact. The variations in each of the parameters was achieved entirely through control of the epitaxial growth procedure. Over 100 individual cells were fabricated and analyzed for this study.

Epitaxial Layer Growth and Evaluation

The device layers investigated in the study were formed via the atmospheric pressure metalorganic vapor phase epitaxy (APMOVPE) process utilizing the chemical reactants, substrates, and growth conditions listed in Table I. A specially designed crystal growth system was constructed for this purpose with several important features. The gas handling system was composed of interior-electropolished 316 stainless steel tubing connected by a combination of leak-tight welded, VCR and O-ring fittings with electronic mass flow controllers for metering and controlling the source gas flow rates. The system is a run/vent type utilizing a split main mixing manifold composed of a series/parallel combination of air-operated 3-port and 4-port bellows valves. The term "split" refers to a separation of the organometallic source vapors from the others until just prior to introduction into the reactor vessel. Such a manifolding arrangement allows for fast gas switching times and also reduces the possibility of homogeneous or heterogeneous reactions in the vapor phase preceding InP growth. Palladium-diffused hydrogen is used as the carrier gas throughout the system. A high-performance quartz reactor vessel capable of producing highly uniform epilayers was used, the design details of which are described elsewhere [ref. 4]. Water cooling of the reactor vessel walls served to condense excess phosphorus from the growth process and confined it to the upper portions of the reactor. This, combined with a helium purging sequence, essentially eliminated the problems of spontaneous ignition of the phosphorus when the reactor was opened to air for loading or unloading wafers. Experience has shown that water-cooled and air-cooled reactor vessels yield epilayers with similar properties. A susceptor, composed of uncoated high-purity graphite and heated by radio frequency induction, was used. The substrate temperature was measured using a thermocouple inserted within the susceptor with temperature stability achieved via a feedback power controller for the RF generator.

The substrates used in this process were single-crystal, liquid encapsulated Czochralski (LEC) InP and were delivered polished on one side and etched on the other from each of the vendors listed in Table I. Wafers were loaded into the reactor as received without any further preparation. Prior to growth, the substrates were heated to 700°C for five minutes with phosphine flowing to the reactor from a cold start. The temperature was then lowered and stabilized at 650°C and the desired mole fractions of $(CH_3)_3In$ and $(C_2H_5)_2Zn$ were then introduced to the run stream to commence the growth of p-type InP. The thickness of the individual epilayers was assumed to be equal to the growth time multiplied by the calibrated growth rate determined from measurements on thicker layers. In the case of p-type layers, the desired impurity concentration was achieved in two different ways depending upon the desired level. For $(N_A - N_D) > 1 \times 10^{17} cm^{-3}$ the doping was obtained through the usual manner of bubbling through the source, while for $(N_A - N_D) < 1 \times 10^{17} cm^{-3}$ a special controlled source evaporation technique was employed. Impurity concentrations for the n- and p-type layers were verified using capacitance-voltage measurements on finished cells with one-sided n^+/p junctions or with similar measurements using a mercury probe on single layers. Formation of the n^+/p homojunction was achieved by simultaneously stopping the $(C_2H_5)_2Zn$ flow and introducing H_2S, with the emitter thickness being equal to the time from the introduction of the H_2S to the termination of growth, multiplied by the calibrated growth rate. Generally, the surface morphology and overall epilayer quality was ostensibly the same for substrates obtained from each of the vendors.

Solar Cell Fabrication

Following growth, the device wafers were processed into arrays of electrically isolated solar cells with the cell areas and grid contacts defined using standard photolithographic and chemical etching techniques. Mesa cells 0.10 cm^2 in area with a nominal grid coverage of 10% were formed by etching orthogonal isolation troughs with 9 H_3PO_4:1 HCl at room temperature. The top grid contacts were formed by electroplating pure Au to the n$^+$ layer while the back contact was formed by sintering a 1500Å thick layer of evaporated Au/Be in flowing forming gas at 400°C for 1 minute and then overplating with ~2 μm of pure Au. This process yielded seven to twelve finished solar cells on each device wafer. For the purposes of the study, antireflection coatings (ARC) were not applied to the cells in order to keep the analysis of the results as simple as possible. However, after analyzing the results, a few cells with near-optimum design parameters had a two-layer ARC of ZnS/MgF$_2$ applied. The individual thicknesses of these were determined using a recently developed two-layer coating optimization technique.

Results and Discussion

Performance of the shallow-homojunction cells was characterized using dark J-V, light J-V and spectral response techniques. For comparison purposes, the light J-V data were obtained under standard global conditions at 25°C with total irradiance of 1000 Wm^{-2} and using total cell area [ref. 5]. The quantum efficiency was calculated using active area. For the better cells which had a two-layer ARC applied a light J-V measurement under AM0 conditions was also performed using total cell area, a junction temperature of 25°C and a total irradiance of 1367 Wm^{-2}. The measurement uncertainty for each of the global and AM0 conversion efficiency measurements is $\pm 2\%$.

The variation of cell performance parameters with nominal emitter thickness is given in Figure 2 for cells with emitter and base doping concentrations held constant at $N_D = 4 \times 10^{18}$cm^{-3} and $N_A = 4 \times 10^{16}$cm^{-3}, respectively. The data indicate a strong steady increase in J_{sc} as the emitter thickness is reduced from 700Å to 200Å. Figure 3 shows a composite of internal quantum efficiency curves for the same devices indicating a decrease in overall response as the emitter thickness increases, particularly in the blue. Returning to Figure 2, V_{oc} and FF remain roughly constant with emitter thickness down to 200Å showing only slight fluctuations which are thought to be due to minor, unintentional variations in the growth and processing procedures from run to run. Thus, for emitter thicknesses > 200Å, the conversion efficiency dependence on the emitter thickness is dominated by the behavior of the quantum efficiency. The decrease in photocurrent results from increasing recombination losses at the surface, and within the bulk, of the heavily doped emitter layer as the thickness is increased. For emitter thicknesses < 200Å, however, the performance parameters, particularly V_{oc} and FF, decrease dramatically resulting in a significant drop in the conversion efficiency. A similar behavior has been observed in our laboratory for shallow-homojunction cells fabricated in other III-V materials such as GaAs[ref. 6] and GaAs$_{0.74}$P$_{0.26}$. In all cases, the catastrophic failure of the cells correlates well with a dramatic increase in the dark reverse saturation current for junctions with emitters thinner than the critical value. However, the physical mechanism(s) responsible for the increase have not been identified as yet. Surface recombination effects and "narrow" diode behavior are possible causes. In any case, the peak efficiency occurring for an emitter thickness in the 200–300Å range is a direct consequence of these effects and represents an intrinsic limiting factor for the shallow-homojunction cell performance.

The effects of varying the base doping concentration are summarized in Figure 4. In this case, the emitter thickness and doping concentration were held constant at 400Å and $N_D = 4 \times 10^{18} cm^{-3}$, respectively. V_{oc} and FF each tend to improve as the base doping concentration is increased and this trend is consistent with an increasing value of the product $N_A N_D$ and a decreasing recombination component of the dark current due to a decreasing depletion width. J_{sc} , however, remains relatively constant as the base doping concentrations increased up to a value of $6 \times 10^{16} cm^{-3}$, and decreases thereafter. Internal quantum efficiency curves for the same cells are compared in Figure 5 and show that the red response decreases for the higher values of base doping concentration indicating that the minority carrier diffusion length and lifetime are insufficient for the higher values. The combined effects of the variations in V_{oc} , J_{sc} and FF result in the conversion efficiency reaching a maximum for a base doping concentration of about $5 \times 10^{16} cm^{-3}$. Thus, the optimum values for the emitter thickness (200-300Å) and base doping concentration ($\sim 5 \times 10^{16} cm^{-3}$) are in agreement with those predicted by Goradia et al. in a recent modeling study [ref. 3].

The cell performance dependence on emitter doping concentration is illustrated in Figures 6 and 7. The emitter thickness was held constant at a higher-than-optimum value (700Å) to see more clearly the doping effect whereas the base doping concentration was held at $4 \times 10^{16} cm^{-3}$. V_{oc} and FF show a monotonic increase with increasing emitter doping which is due presumably to a lower emitter sheet resistance, an increasing value of $N_A N_D$ and a decreasing recombination current component from the emitter. A monotonic decrease in both J_{sc} and the internal quantum efficiency red response is observed as the emitter doping increases indicating that the minority carrier diffusion length and lifetime are insufficient at higher emitter doping levels. The opposing trends in V_{oc} , FF versus J_{sc} tend to compensate one another and result in the conversion efficiency showing little variation with emitter doping, at least for the emitter thickness of 700Å used here. For thinner emitters, the overall effect on conversion efficiency may be quite different and further work should be performed in this regard.

The better junctions in this work, had ideality factors (n) and reverse saturation current densities (J_0) of $1.03 < n < 1.08$ and $1 - 2 \times 10^{-13} mA \, cm^{-2}$, respectively. Cells with emitters $<$ 200Å thick or bases with $< 2 \times 10^{16} cm^{-3}$ impurity concentration had larger values of both n and J_0 . Although a detailed analysis of the latter variations has not been performed, it seems likely that excessively thin emitters cause enhanced surface recombination while lightly doped bases cause enhanced recombination in the space charge region. In addition, a larger diffusion current would be expected due to the lower built-in potential of the cells with lightly doped bases.

Using the information derived from this work, a few cells with near-optimum design parameters were fabricated to test our conclusions. The cells had a total area of 0.108 cm^2, 5% grid coverage, a 2-layer ARC of ZnS/MgF$_2$ with a structure consisting of a 0.5 μm buffer layer doped to $5 \times 10^{18} cm^{-3}$, a 3 μm base layer doped to $5 \times 10^{16} cm^{-3}$, and a 250Å emitter layer doped to $4 \times 10^{18} cm^{-3}$. Performance data for one of the better cells are given in Figures 8 and 9. The achievement of global and AM0 conversion efficiencies of 20.3% and 17.6%, respectively, demonstrate the success of the study, however further improvements in cell performance should be possible. The internal quantum efficiency data indicate that substantial gains in J_{sc} can be made, particularly in the blue, and we feel that improved grid designs and emitter layer properties will lead to values of J_{sc} under global conditions in the 29-30 mA cm^{-2} range. Furthermore, a degradation of the junction dark J-V characteristics, illustrated in Figure 10, was observed after deposition of the ZnS component of the

two-layer ARC. J_0 increased by an order of magnitude and n by ~10% which we estimate lowered V_{oc} by about 4 mV. The degradation is believed to be due to either a shunting path formed by the ZnS deposition along the edge of the cell mesa or to cell damage occuring during the electron-beam evaporation coating process. Revised processing procedures are being developed to address this problem. Finally, improved values for FF are possible since we have already observed values as high as 86% for similar cells fabricated in our laboratory. Therefore, a realistic upper limit for the conversion efficiency using the present structure appears to lie in the 21-22% range. The results obtained so far are particularly encouraging considering that the epilayers were formed using a simple growth procedure at atmospheric pressure with a relatively low V/III ratio.

Conclusions and Future Directions

The emphasis in this work to-date has been on an empirical investigation of the effect of the cell design parameters on performance. Devices with efficiencies > 20%, measured under standard global conditions, have been achieved and the trends in device behavior with emitter and base doping and emitter thickness are in general accordance with expectations from elementary theory. The key conclusions which can be drawn from the work are:

1. Of the three variables investigated, the dominant influence is the emitter thickness. The cell efficiency increases monotonically with decreasing emitter thickness but decreases catastrophically at a thickness of < 200Å. This effect is unlikely to be due to morphological shortcomings and its origins remain to be determined. It should be pointed out that elementary theory does not incorporate this effect.

2. Further improvements in device efficiency are likely to result from a thorough investigation of the factors influencing V_{oc} and from an improvement in the blue response. These will result from improved materials properties and cell design.

Improvements in efficiency towards the goal of a device with an AM0 efficiency of > 20% are likely to result from both fundamental and technological developments. Under the classification of fundamental aspects, the following can be included.

1. More attention must be paid to the level of emitter doping and the possibility of establishing an emitter doping profile. Equally, the optimum thickness of the base is not yet established although preliminary data on this are now available.

2. It is essential to establish the variation of epilayer quality as a function of that of the substrate. Therefore an assessment of wafer quality from a range of different vendors using a variety of optical and structural characterization techniques should be performed.

3. Little work has yet been undertaken on optimizing the growth parameters (e.g., temperature and V/III ratio) of the epilayers to achieve improved materials properties. Although the materials properties seem excellent, significant improvements may result from this. Preliminary investigations of dark current mechanisms imply a significant contribution from space charge recombination through near mid-gap states. Attempts are presently being made to correlate these data with DLTS measurements and, together, this information may influence the selected growth conditions.

4. Preliminary device modeling has been performed but reveals a shortage of accurate values for input parameters. Hence, it is essential to perform independent measurements of lifetimes, diffusion lengths and surface recombination velocity. None of these is presently well established for these devices.

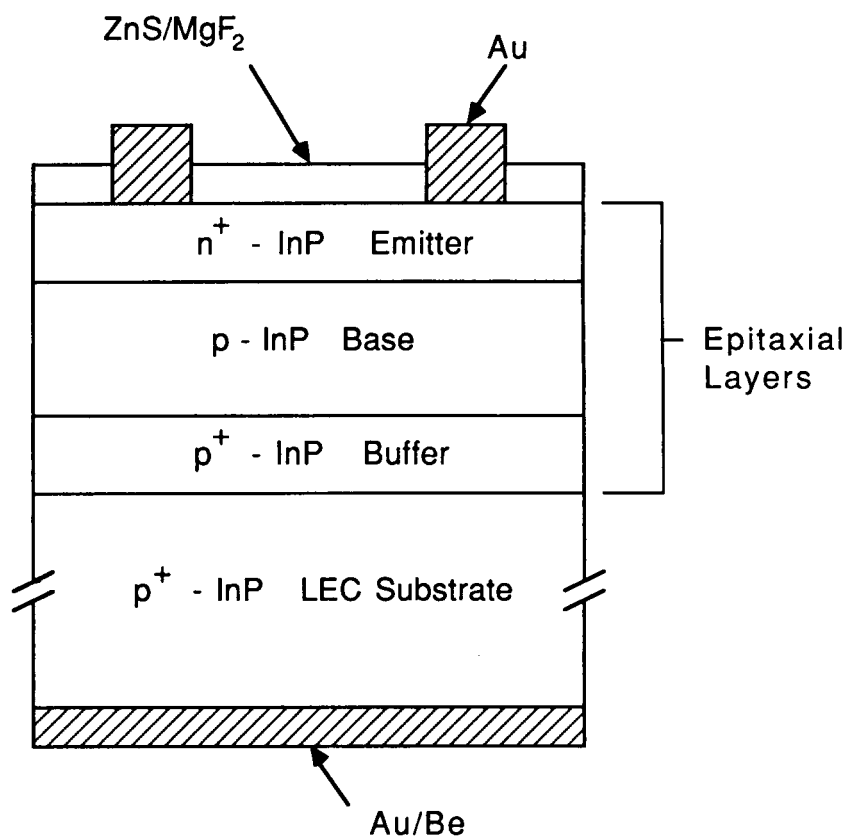Under the category of technological aspects can be included:

1. Since device efficiencies are now within 2% of the theoretical maximum, it is suggested that significant improvements may result from a scale up in the size and number of devices produced. It is believed that this will lead to refinements in and better understanding of the growth procedure and device processing.

2. It is also essential to produce larger area devices including standard space cell size for realistic measurements of radiation resistance and the modification of design aspects such as the grids. Larger area devices will also reduce the effects of leakage at the perimeter of the devices through a reduction in the ratio of perimeter to surface area. In addition, the growth of large area devices is sure to introduce new problems which should be investigated sooner rather than later.

3. Studies of grid adhesion and back-contact stability are also an imperative and should be initiated as soon as possible.

References

[1] M. Yamaguchi, K. Ando, A. Yamamoto and C. Uemure, Appl. Phys. Lett., 44, 432 (1984).

[2] M. B. Spitzer, C. J. Keaveney, S. M. Vernon and V. E. Haven, Appl. Phys. Lett., 51, 364 (1987).

[3] C. Goradia, J. V. Geier and I. Weinberg, *Proc. 19th IEEE Photovoltaic Specialists Conference*, New Orleans, Louisiana, (1987), p. 937.

[4] M. W. Wanlass, U.S. Patent No. 4,649,859.

[5] "Standard Test Methods for Electrical Performance of Non- Concentrator Terrestrial Photovoltaic Cells Using Reference Cells," ASTM Standard E948.

[6] A. E. Blakeslee, H. Aharoni, M. W. Wanlass, A. Kibbler, K. Emery and C. R. Osterwald, *Proc. 18th IEEE Photovoltaic Specialists Conference*, Las Vegas, Nevada, (1985), p. 146.

TABLE I. A summary of the chemical reactants, substrates, and growth conditions used in the APMOVPE process

Chemical Reactants

Reactant	Application	Vendor
Trimethylindium $[(CH_3)_3In]$	In Source	Alfa Products
Phosphine $[PH_3]$	P Source	Phoenix Research
Diethylzinc $(C_2H_5)_2Zn)$	Zn Source (p-doping)	Alfa Products
500 ppm Hydrogen Sulfide in Hydrogen $[500$ ppm $H_2S/H_2]$	S Source (n-doping)	Scientific Gas

Substrates

Vendor	Orientation	Dopant	Carrier Concentration
ICI Americas Inc.	(100)	Cd	1.7×10^{18} cm^{-3}
Sumitomo Electric Industries, Ltd.	$(100) \pm 0.5°$	Zn	4.1×10^{18} cm^{-3}
Nippon Mining Co., Ltd.	$(100)2°\rightarrow(110)\pm0.09°$	Zn	4.3×10^{18} cm^{-3}

Growth Conditions

Parameter	Value
Reactor Pressure	640 mm Hg
Growth Temperature	650°C
Growth Rate	6 μm hr^{-1}
H_2 Carrier Flow Rate	3000 sccm
Group V/Group III in Vapor	33.9
$(CH_3)_3In$ Mole Fraction	2.2×10^{-4}

ZnS/MgF$_2$

Au

n$^+$ - InP   Emitter

p - InP   Base

p$^+$ - InP   Buffer

Epitaxial Layers

p$^+$ - InP   LEC Substrate

Au/Be

Figure 1. Schematic cross section of the n$^+$/p/p$^+$ InP shallow-homojunction cell structure under investigation.
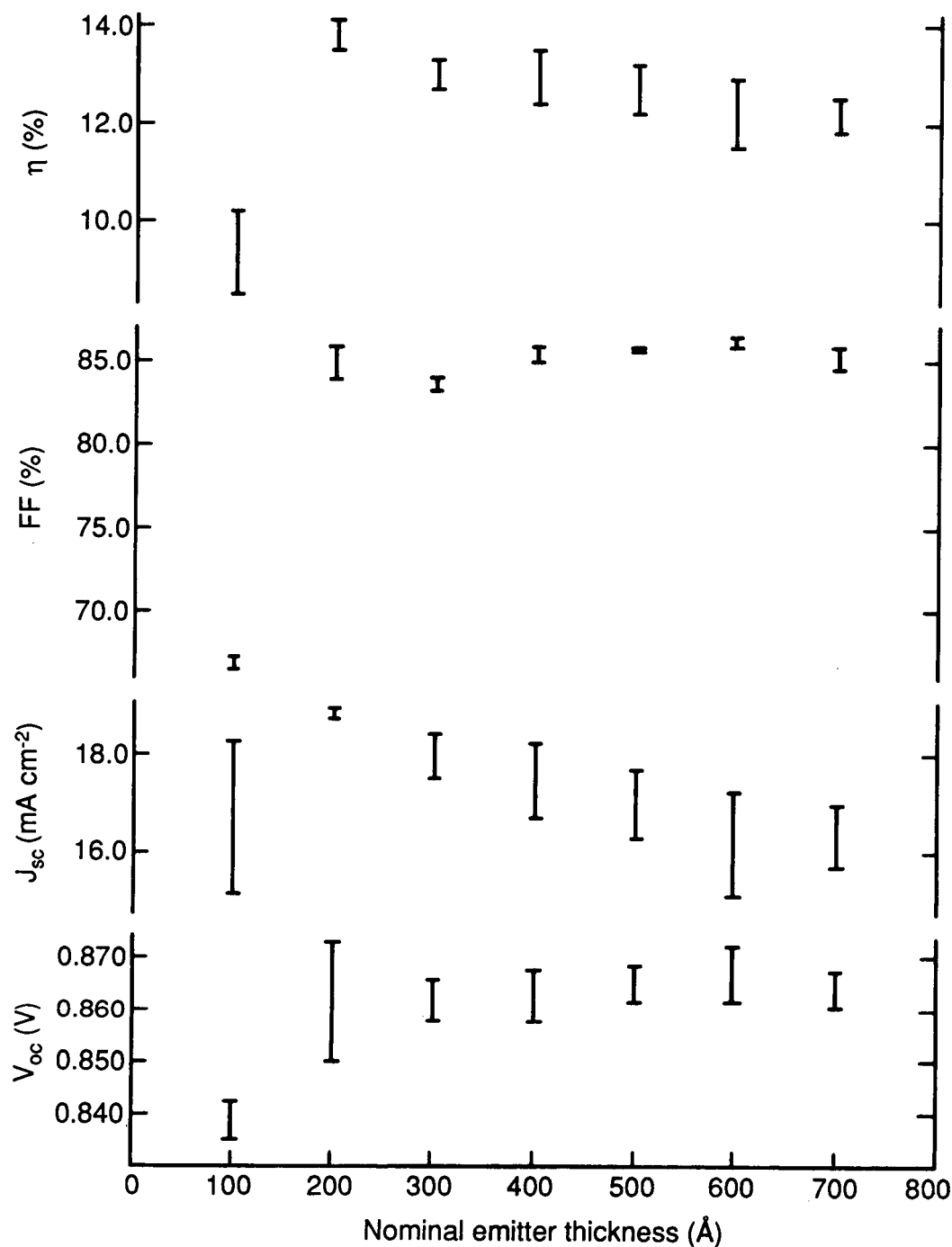
Figure 2. Variation of cell performance parameters Voc, Jsc, FF, and η with nominal emitter thickness. The emitter and base doping concentrations were held constant at N_D = 4×10^{18} cm^{-3}, and N_A = 4×10^{16} cm^{-3}, respectively. The bars indicate the range of values observed on each device wafer.
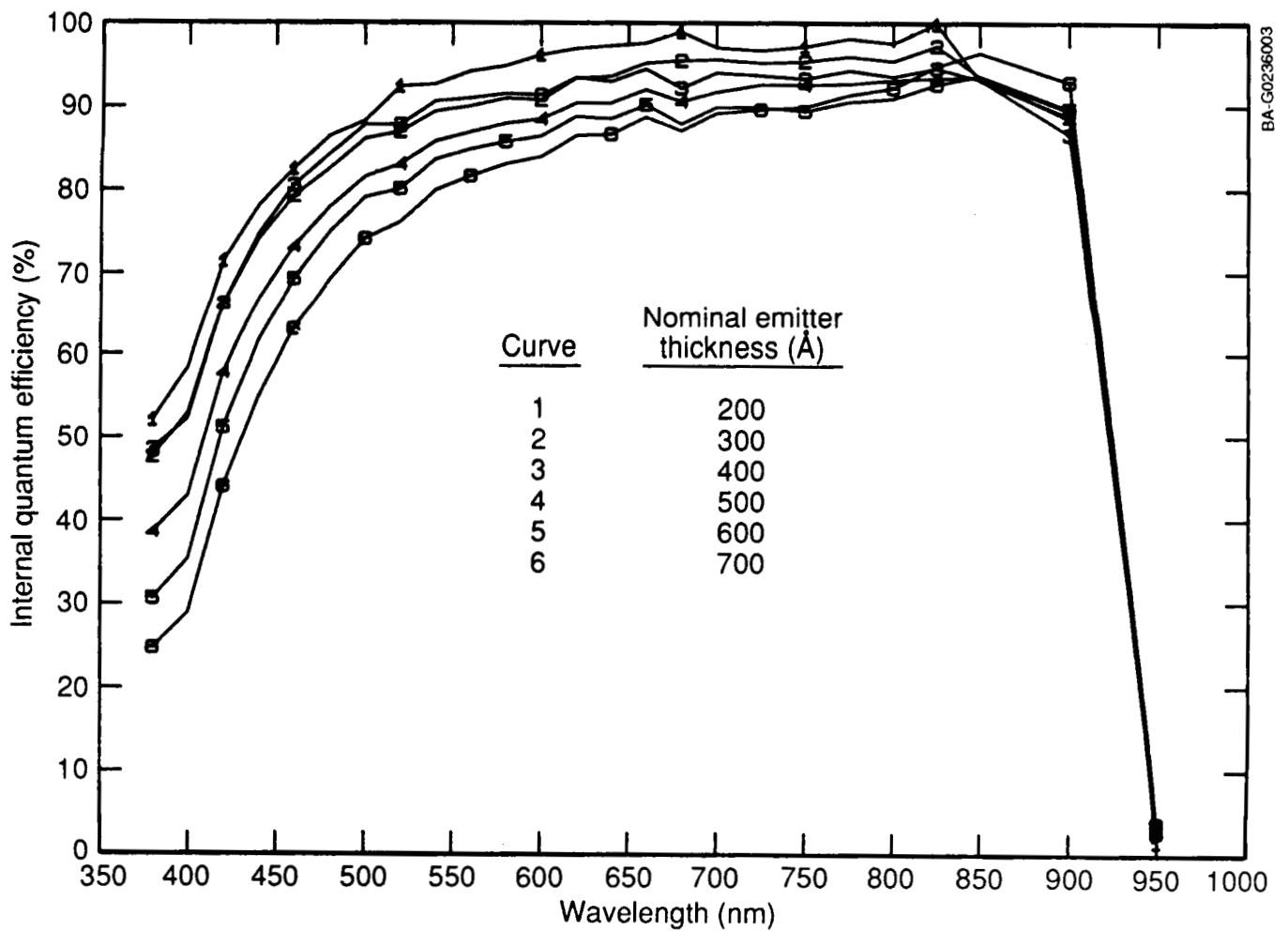
Figure 3. Internal quantum efficiency versus wavelength for different nominal emitter thicknesses showing a decrease in overall response as the thickness increases, particularly in the blue. These curves correspond to devices with parameters shown in Figure 2.
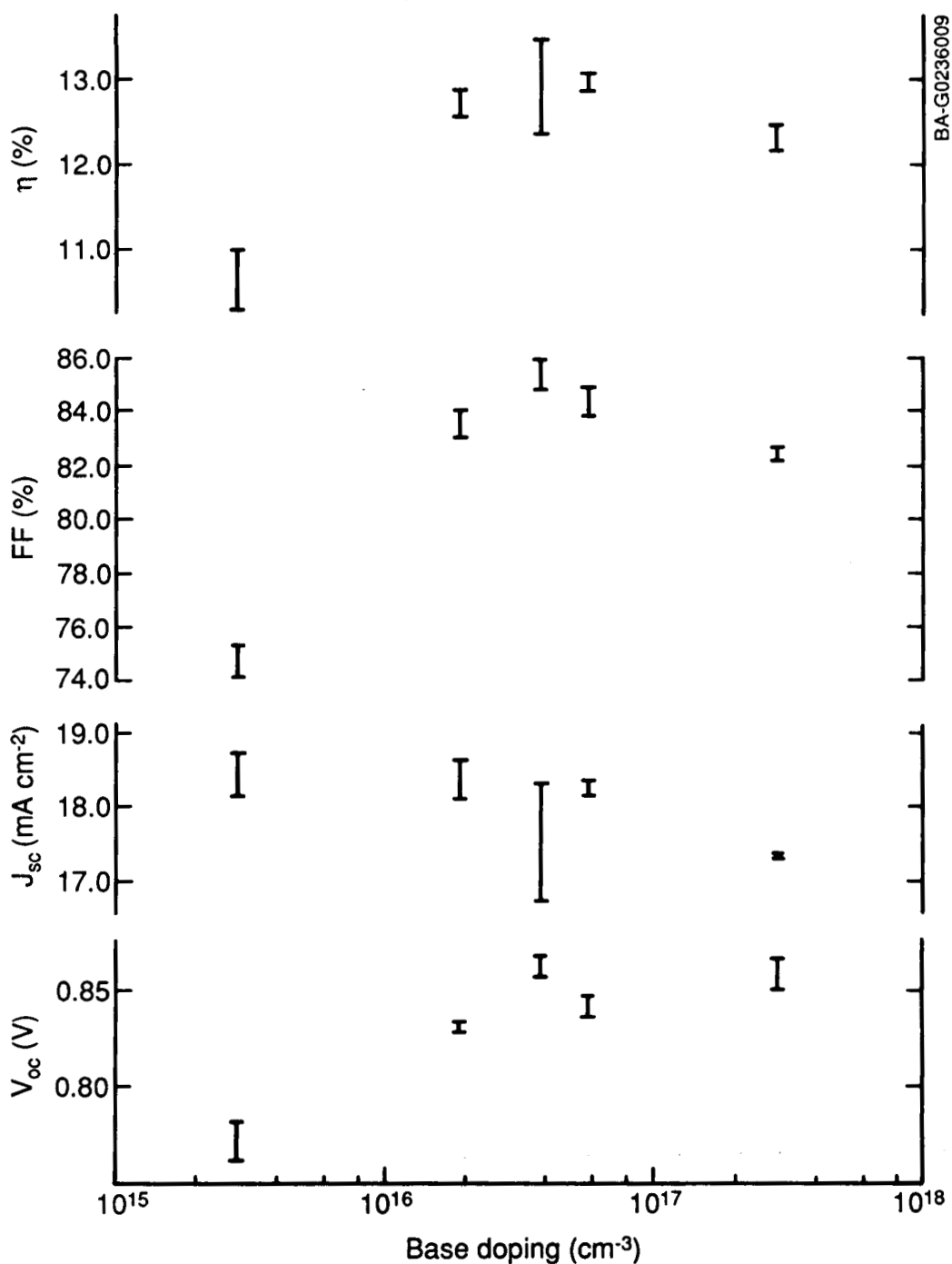
Figure 4. Variation of cell performance parameters Voc, Jsc, FF, and η with base doping concentration. The emitter thickness and doping concentration were held constant at 400 Å and $N_D = 4 \times 10^{18}$ cm^{-3}, respectively. The bars indicate the range of values observed on each device wafer.
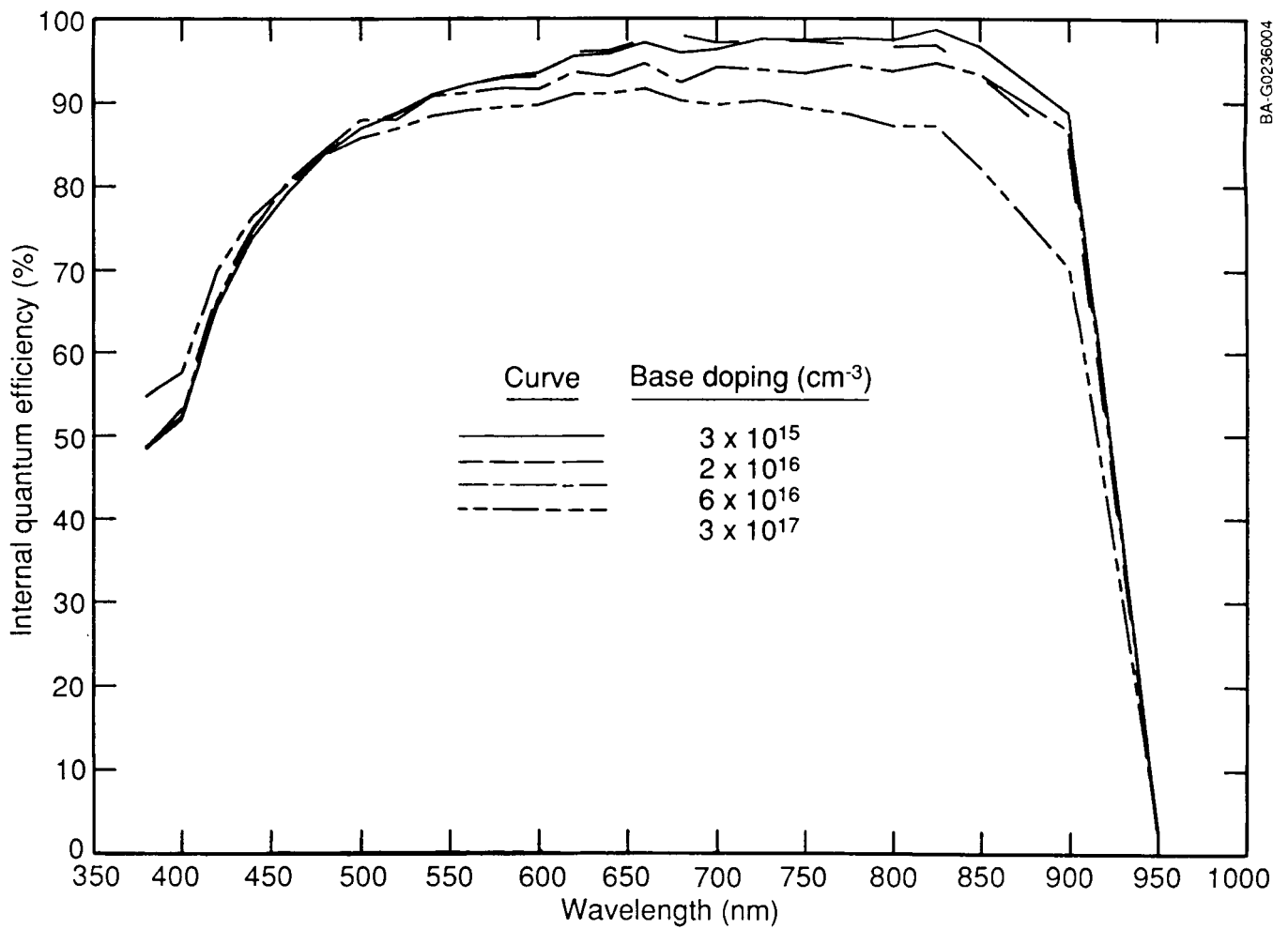
Figure 5. Internal quantum efficiency versus wavelength for different base doping concentrations showing a strong decrease in the red response as the doping concentration is increased beyond 6×10^{16} cm^{-3}. These curves correspond to devices with parameters shown in Figure 4.
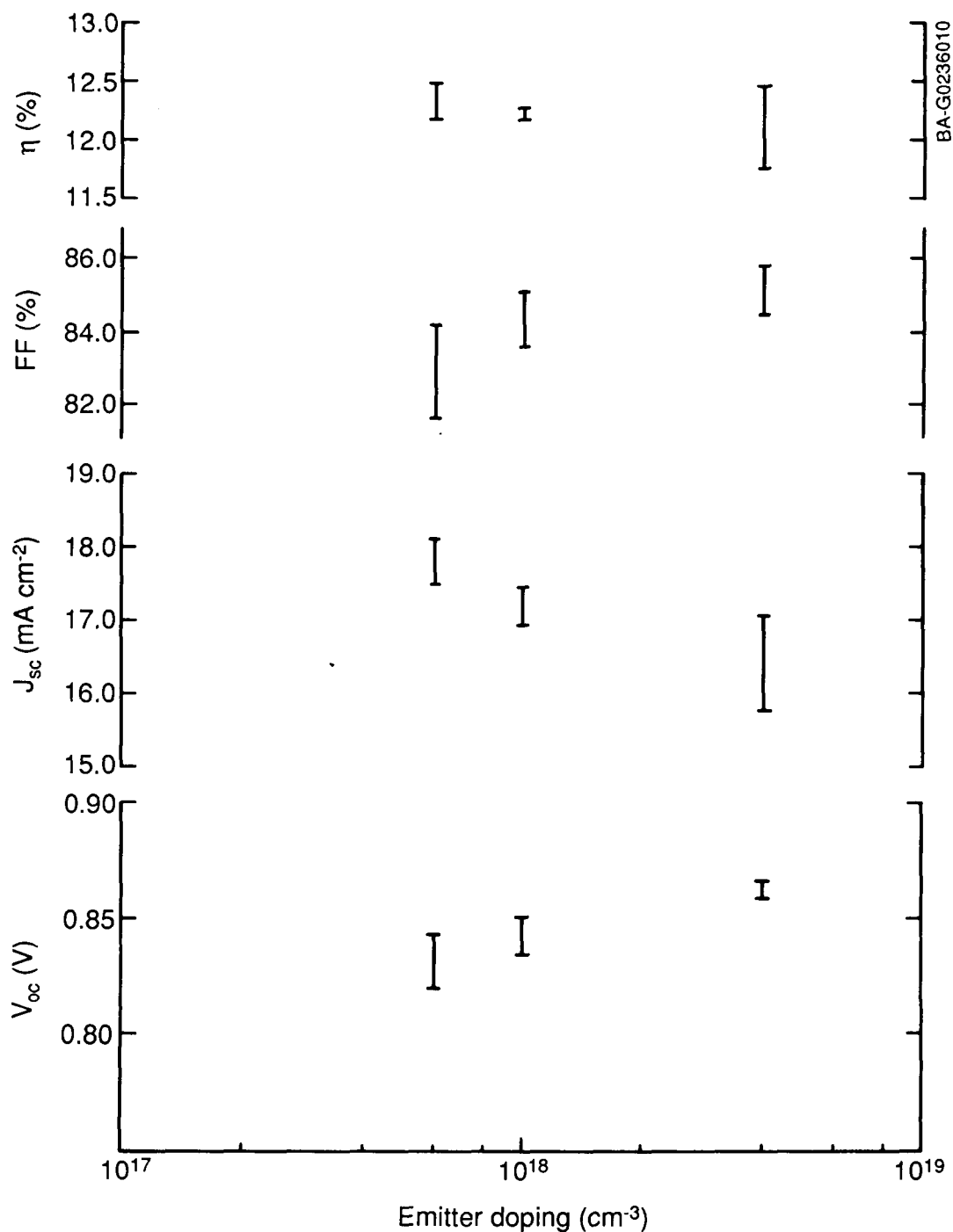
BA-G0236010

Figure 6. Variation of cell performance parameters Voc, Jsc, FF, and η with emitter doping concentration. The emitter thickness and base doping concentration were held constant at 700 Å and $N_A = 4 \times 10^{16}$ cm^{-3}, respectively. The bars indicate the range of values observed on each device wafer.
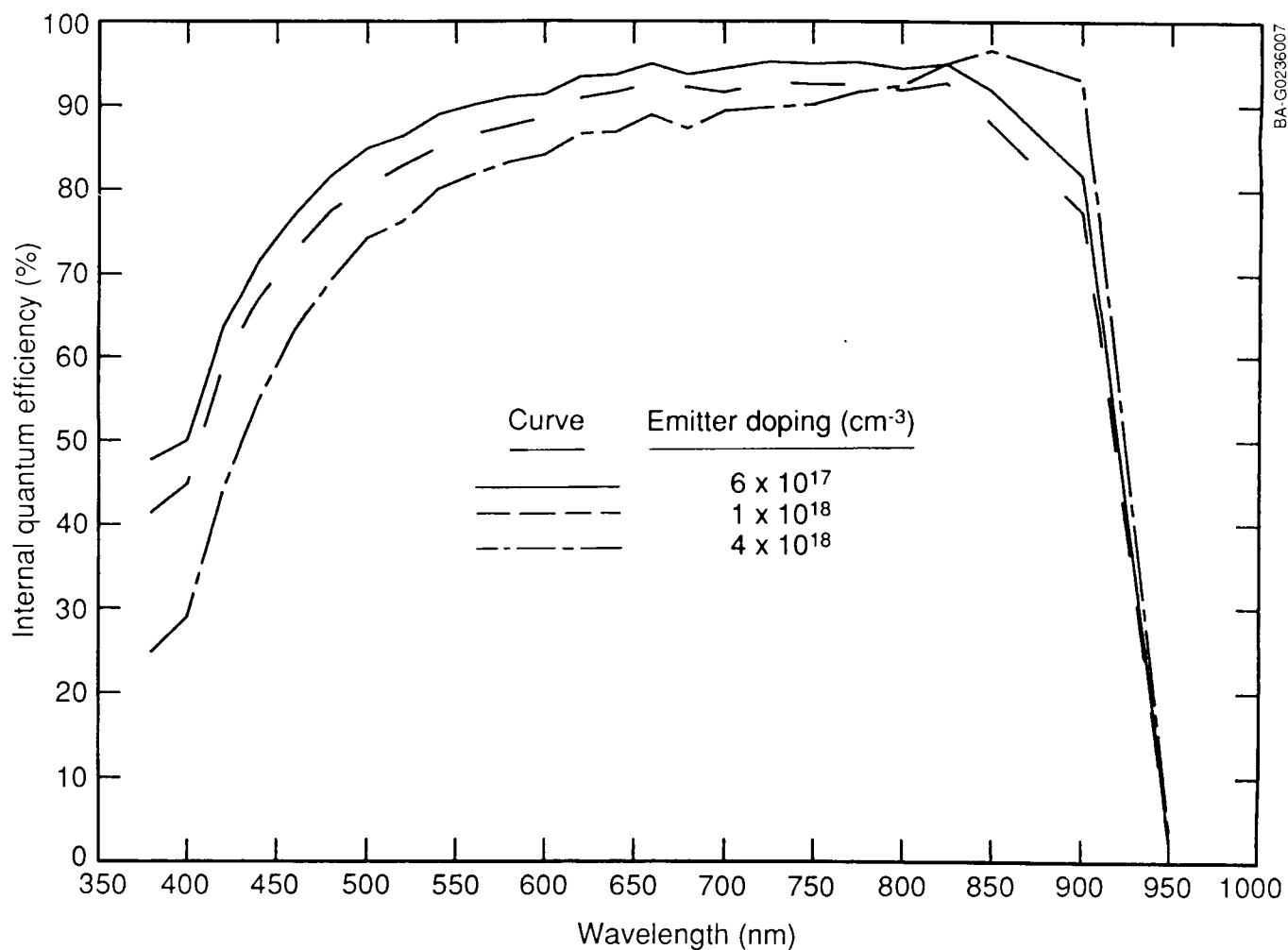
Figure 7. Internal quantum efficiency versus wavelength for different emitter doping concentrations showing a substantial decrease in blue response as the doping concentration is increased. These curves correspond to devices with parameters shown in Figure 6.
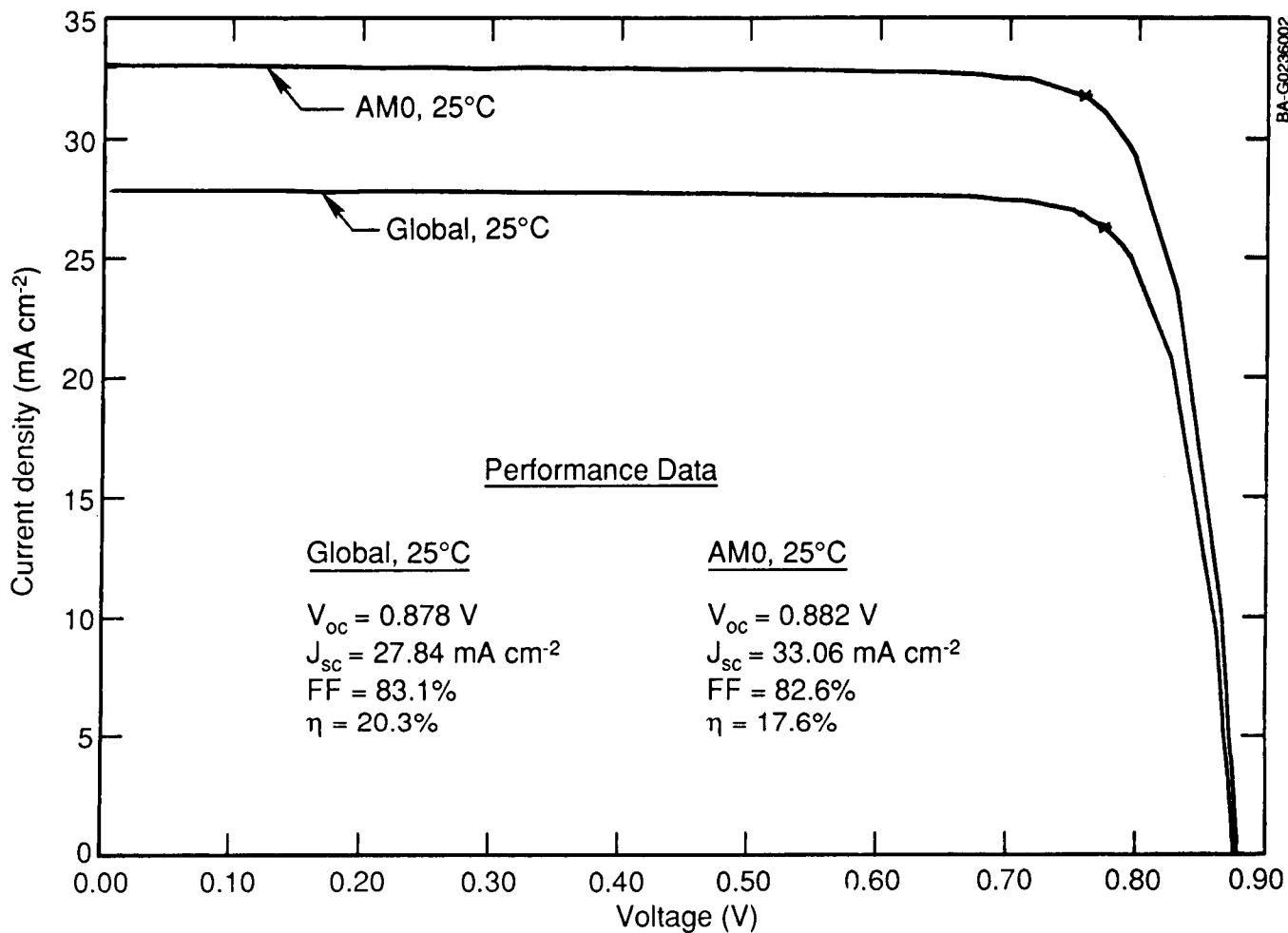
The figure shows Light J-V characteristics with axes "Current density (mA cm^{-2})" from 0 to 35 and "Voltage (V)" from 0.00 to 0.90. Two curves are labeled "AM0, 25°C" and "Global, 25°C".

Performance Data

Global, 25°C

V_{oc} = 0.878 V
J_{sc} = 27.84 mA cm^{-2}
FF = 83.1%
η = 20.3%

AM0, 25°C

V_{oc} = 0.882 V
J_{sc} = 33.06 mA cm^{-2}
FF = 82.6%
η = 17.6%

BA-G0236002

Figure 8. Light J-V characteristics for a near-optimum $n^+/p/p^+$ InP shallow homojunction under global and AM0 illumination at 25°C. The cell performance data for each case are also shown. The cell has a 2-layer antireflection coating of ZnS/MgF_2.
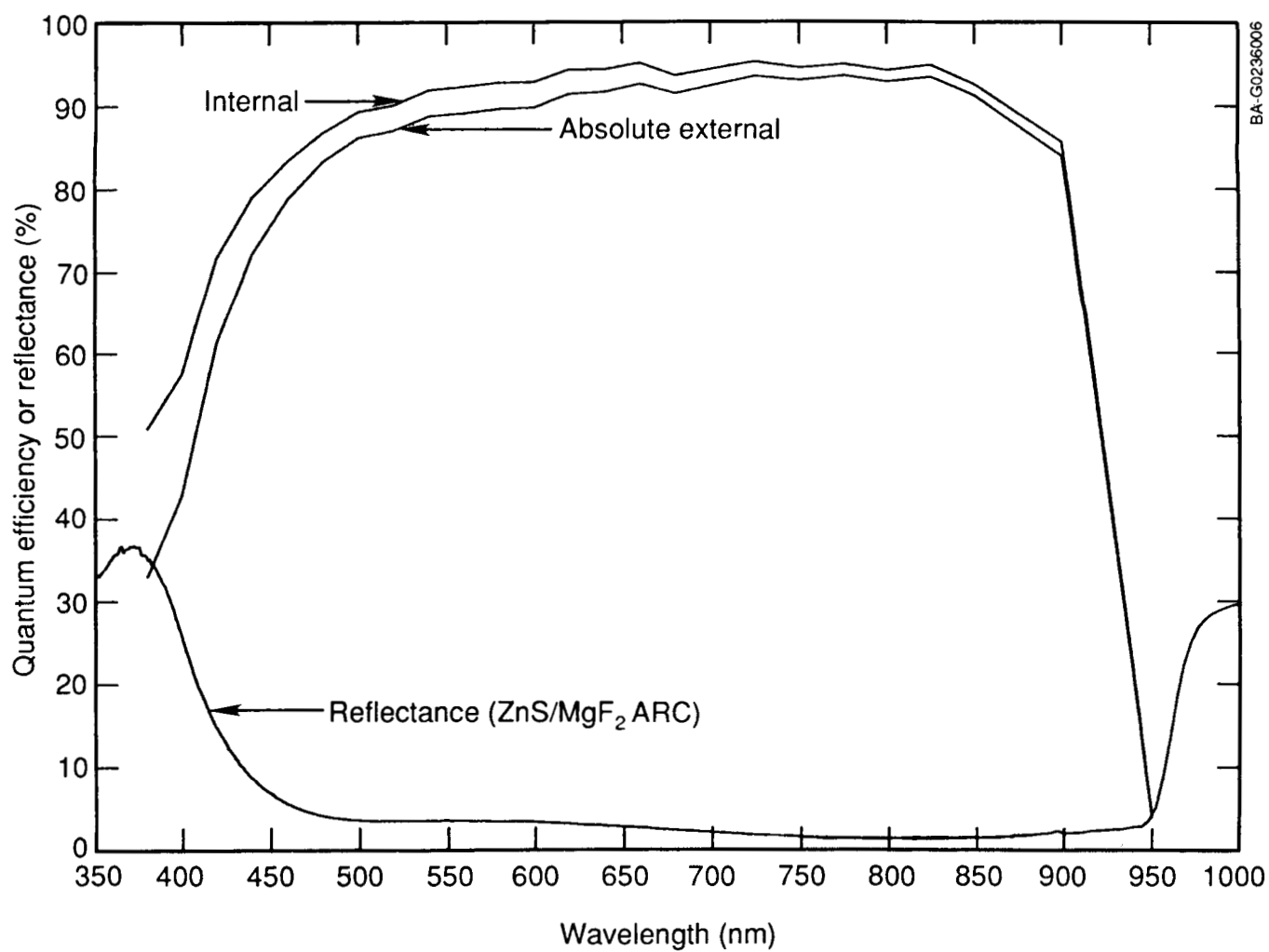
55

Figure 9. Internal quantum efficiency, absolute external quantum efficiency and reflectance data for the cell of Figure 8.
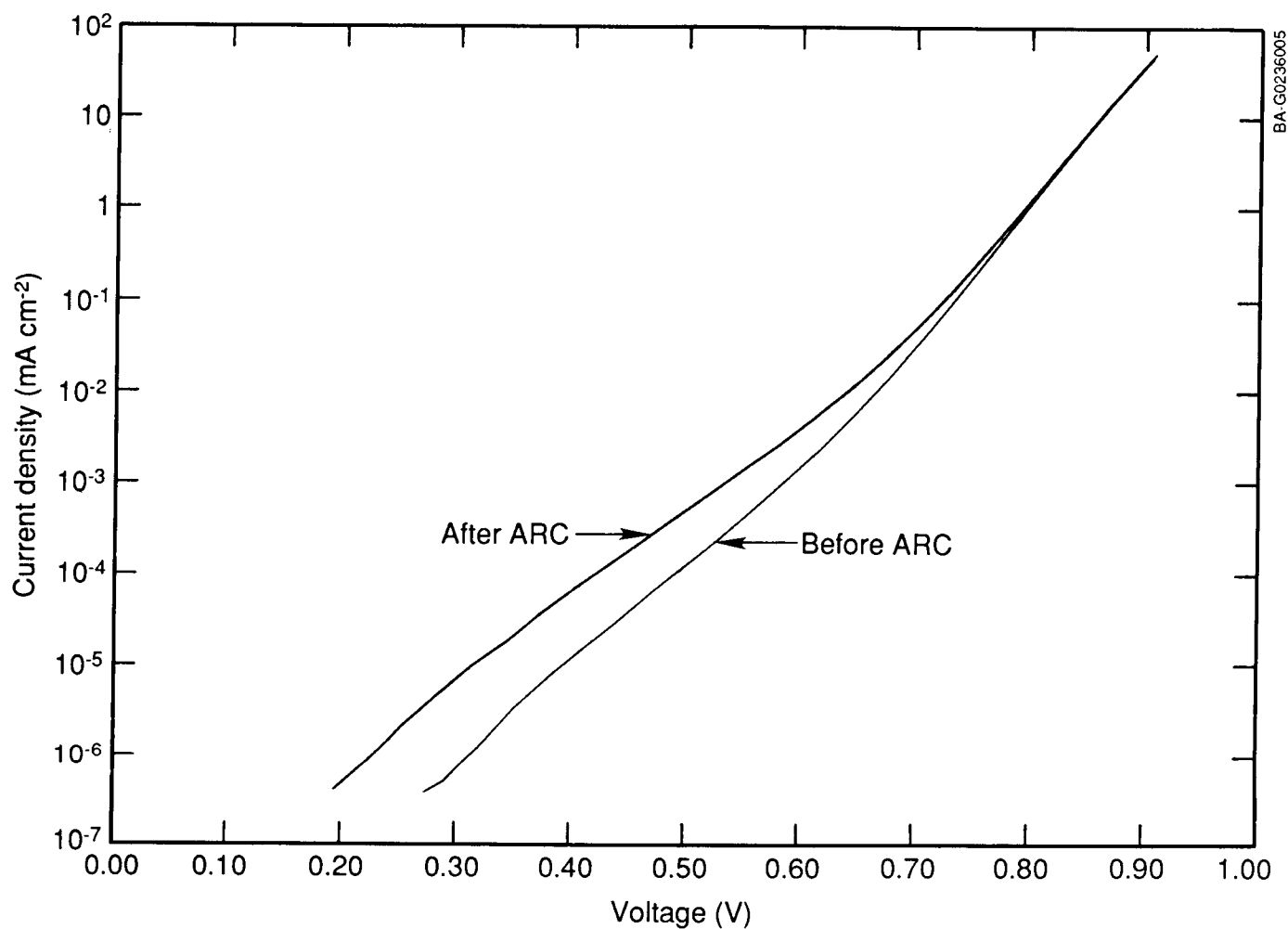
Figure 10. Forward-bias dark J-V data for a high-performance InP cell before and after deposition of the ZnS component of the 2-layer antireflection coating. Note the slight degradation of the characteristic after the ZnS deposition.